Nuclear Inst. and Methods in Physics Research B 441 (2019) 8–11

Contents lists available at ScienceDirect

Nuclear Inst. and Methods in Physics Research B

journal homepage: www.elsevier.com/locate/nimb

Characterization of oxygen self-diffusion in TiO_2 resistive-switching layers by nuclear reaction profiling

M.C. Sulzbach[a,b], F.F. Selau[a,*], H. Trombini[a], P.L. Grande[a], G.G. Marmitt[a], L.G. Pereira[a], M. Vos[c], R.G. Elliman[c]

[a] Ion Implantation Laboratory, Institute of Physics, Federal University of Rio Grande do Sul, Av. Bento Gonçalves 9500, CP 15051, CEP 91501-970 Porto Alegre, RS, Brazil
[b] Institut de Ciencia de Materials de Barcelona (ICMAB-CSIC), Campus de la UAB, 08193 Bellaterra, Spain
[c] Electronics Materials Engineering, Research School of Physics and Engineering, The Australian National University, Canberra 0200, Australia

ARTICLE INFO

Keywords:
Resistive memories
Diffusion mechanisms
Nuclear Reaction Analysis
Conducting filaments

ABSTRACT

Oxygen self-diffusion was investigated in TiO_2 layers employed for resistive-switching memories using resonant nuclear reaction profiling (NRP) and ^{18}O labeling. The layers were grown using physical vapor deposition technique (sputtering) and were polycrystalline. The diffusivity was measured over the temperature range 600–800 °C and the activation energy for oxygen self-diffusion in sputter-deposited TiO_2 films determined to be 1.09 ± 0.16 eV, a value consistent with results obtained by previous studies (Marmitt et al., 2017).

1. Introduction

The search for new memory technologies has increased considerably in the last years. The so-called Resistive Random Access Memories (ReRAMs) have emerged as potential substitutes for conventional flash memory due to its fast write speed, high read/write cycle endurance and low-power consumption. In the case of Valence Change Memories (VCM), the mechanism responsible for the resistance change is electric-field induced diffusion of oxygen vacancies inside a functional oxide layer. The memory cell has a capacitor-like structure comprising of a metal-oxide-metal structure. Previous studies [2–4] indicate that the oxygen-deficient regions create filamentary conduction paths in the oxide layer. The filament has a larger electron conductivity than stoichiometric TiO_2, thus the resistance of the system decreases. This phenomenon is called switching, since the device changes its resistance from a high state (OFF) to a low state (ON) [2].

This filament formation is caused by the drift and diffusion of oxygen in the dielectric layer and therefore the knowledge of the corresponding activation energy is of fundamental importance. In this work we investigate oxygen diffusion in TiO_2 thin films using ^{18}O labeling and the Resonant Nuclear Reaction Profiling (NRP) technique. A previously used technique, electron Rutherford backscattering (ERBS) [1] minimizes the sample damage but relies on the knowledge of the inelastic mean free path and thickness of the oxide. On the other hand, NRP is a more direct method, where the ^{18}O depth profile is measured with a better depth resolution. In fact, depth profiling of light elements with nm scale resolution is challenging. It is thus important to check that different techniques give similar outcomes. Such a comparison, when successful, increases our confidence in the analysis procedures followed and thus strengthens the foundation of the technique.

2. Experimental procedure

Fig. 1 shows a schematic of the samples used. For the samples A, B and C a platinum bottom electrode was used, taking into consideration it is electrochemically inert and a good electric conductor. In order to promote the adhesion of the platinum on the substrate, a thin titanium layer was deposited first on top of silicon substrate. The electrical behavior of set A, B and C were measured after the deposition of a aluminum top electrode.

A set of samples (D) was used to study the oxygen diffusion with NRP, in which the oxide film was comprised of two layers of TiO_2, each one with a different oxygen isotope, ^{16}O and ^{18}O. The ^{18}O isotope allows quantitative profiling of the oxygen distribution using the nuclear reaction $^{18}O(p, \alpha)^{15}N$. Fig. 1(D) shows the structure of the sample grown to study the temperature dependence of oxygen diffusion. A silicon nitride (Si_3N_4) layer was deposited by plasma-enhanced chemical vapor deposition (PECVD) to avoid oxygen exchange between the atmosphere and the sample during annealing [5]. This layer was not removed to perform the nuclear reaction because it does not affect the

* Corresponding author.
E-mail address: felipe.selau@ufrgs.br (F.F. Selau).

https://doi.org/10.1016/j.nimb.2018.11.026
Received 7 August 2018; Received in revised form 19 October 2018; Accepted 14 November 2018

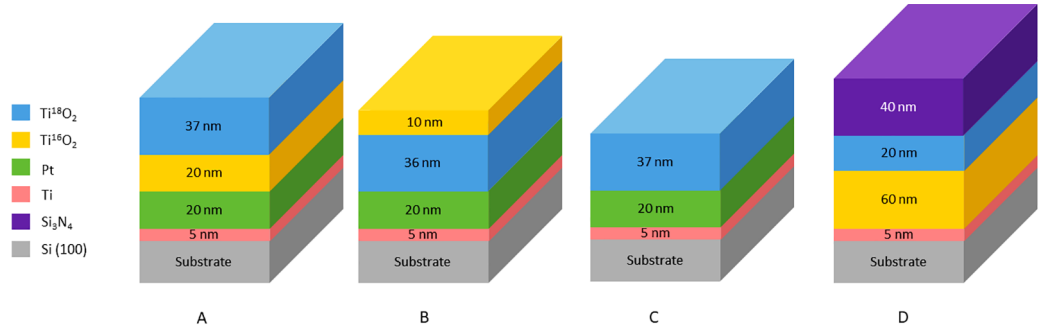

Fig. 1. Sketch of samples studied for oxygen self diffusion in TiO_2. The oxygen profile and the electrical behavior of A, B and C were analyzed. Sample D was produced for diffusion studies.

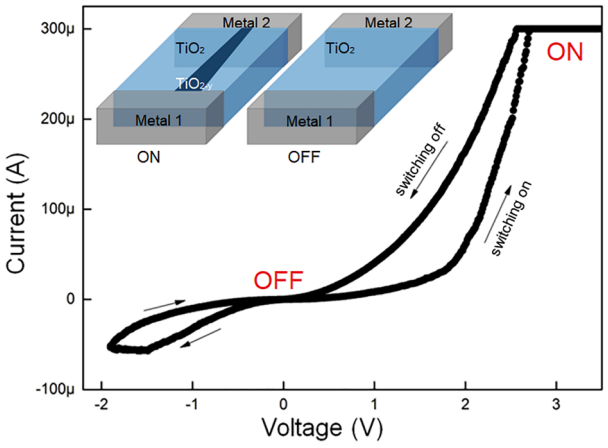

Fig. 2. Electric measurements of sample C after deposition of an aluminum electrode with thickness of 400 nm. The inset shows a sketch of the formation of a filament inside TiO_2, which causes the change in resistance.

final results significantly. In addition, the removal of this layer could introduce additional errors because of its stronger adherence after annealing at high temperatures (> 700 °C). In fact, the annealing at high temperatures changes the (Si_3N_4) density and the layer becomes more resistant to chemical etching. The presence of remaining cap layer with different thicknesses for different annealing temperatures can introduce additional errors since an additional free parameter must be included in the simulation. This is an advantage of the present nuclear reaction over other techniques, such as electron RBS used in [1]. Pieces of the same sample were annealed using Rapid Thermal Annealing (RTA) at 600, 700 and 800 °C for 5 min. The heating causes the mixing of the oxygen isotopes close to the interface between the two layers of TiO_2.

The NRP measurements were performed at the Ion Implantation Laboratory (LII) of the Federal University of Rio Grande do Sul (UFRGS). The beam of H^+ was obtained by a linear 500 keV electrostatic accelerator to induce the nuclear reaction $^{18}O(p, \alpha)^{15}N$, which has a sharp maximum in the across section at an energy of 151 keV with a width of 50 eV [5–7]. During the analysis the energy distribution of the incoming beam and Doppler broadening were taken into account by assuming an overall Gaussian energy-loss fluctuation of FWHM = 130 eV, which is close to the value used in Ref. [7]. Based on this value a depth resolution of 0.7 nm should be attainable very close to the surface. A surface barrier detector with surface area of 1200 mm^2 was positioned at 150° in relation to the incident beam. To avoid detection of backscattered protons from the target, a 10 μm aluminized Mylar absorber foil is positioned just in front of the detector. This foil prevents protons (which have energies about 150 keV) from being detected [8], but does not stop the alpha particles with an energy of the order of 3 MeV (Q value of the reaction is 3.98 MeV) [9]. The resulting excitation curve was analyzed with the PowerMEIS software (available online) [10,11]. This software uses a Monte Carlo algorithm that performs simulations of electron and ion-beam interaction with matter. In these simulations a depth distribution of ^{18}O was assumed. The measured and simulated reaction yield as a function of the incoming beam energy was compared. The oxygen distribution describing the experiment best was obtained through a chi-square (χ^2) analysis from [12].

3. Results and discussions

The samples A, B and C were structured with electrodes of Aluminum and Platinum, which were used to perform the electrical measurements. These measurements showed a typical behavior of a resistive switching device caused by the movement of oxygen vacancies. In Fig. 2 we show the electrical measurements for sample C that displays this behavior.

Nuclear reaction excitation curves, i.e. the alpha yield as a function of the incident proton energy, are shown in Fig. 3 for samples A, B and C. From PowerMEIS simulations of the excitation curve we obtain the thickness of the $Ti^{18}O_2$ layer and estimations from the sharpness of the onset for the corresponding roughness and/or the thickness of overlayer, if present. The $Ti^{18}O_2$ thicknesses are 37, 36 and 37 nm respectively and are shown in Fig. 1. The roughness for samples A and C is less than 0.5 nm, which is smaller than the region where the isotopic exchange (^{18}O by ^{16}O at the surface) takes place and amount according to the sharpness of the onset of about 5 and 2.5 nm for samples A and C respectively. The red lines in Fig. 3 correspond to the simulations based on the parameters described above. In addition they have been taken into account to analyze the effect of the temperature for the oxygen diffusion in sample D. In this way, the parameters of simulation (e.g. stopping power and energy loss straggling) were determined from the best fit in Fig. 3 and kept fixed for the analysis of the annealed samples. The values of stopping power and energy loss straggling agree with ones from SRIM [13] and Chu formula [14] respectively. To investigate the presence of the beam damage induced diffusion, we have monitored the excitation curves as a function of integrated charge as shown in Fig. 4 for samples similar to sample D. It is not possible to note any significant change of the oxygen profile near the interface $Ti^{18}O_2$/$Ti^{16}O_2$ within the statistical errors error. Nevertheless, some changes are observed for ^{18}O inside the cap layer.

The excitation curves are shown in Fig. 5 for each annealing temperature. The measurement was simulated using the PowerMEIS package (Monte-Carlo simulation) which calculates the ^{18}O depth

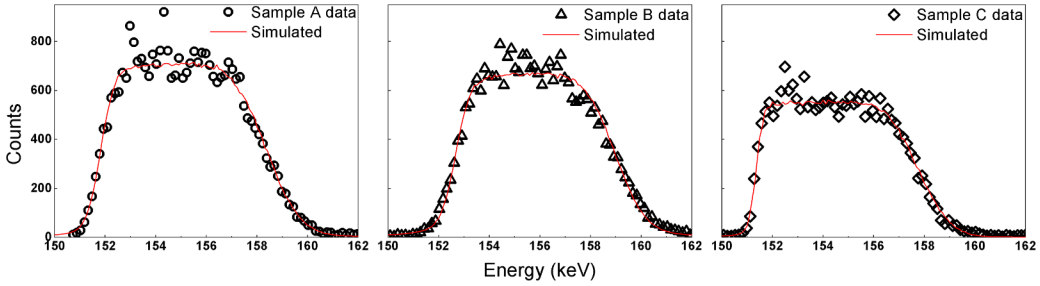

Fig. 3. Excitation curves of ^{18}O measured with nuclear reaction $^{18}O(p, \alpha)^{15}N$ for samples A, B and C.

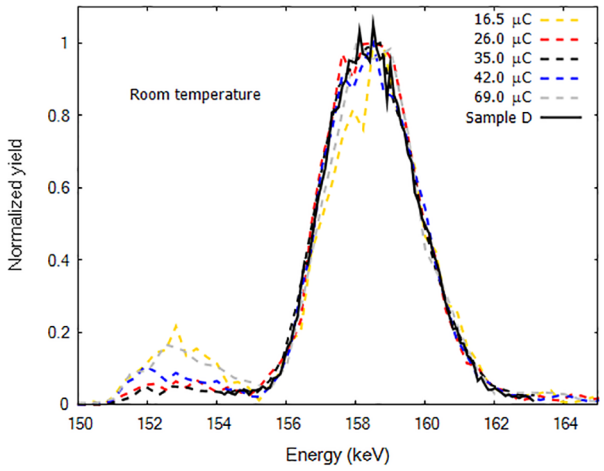

Fig. 4. Experimental excitation curves for protons in non-annealed sample similar to sample D for different fluences ($1\mu C = 2.5 \times 10^{13}$ atoms cm^{-2}). The excitation curve for the non-annealed sample D used for the diffusion experiments is also shown.

distribution for given *Dt* value by solving the one dimension Fick's law of diffusion. The depth resolution (standard deviation) after 40 nm (Si_3N_4) is 4.5 nm and after 40 nm (Si_3N_4)/20 nm $Ti^{18}O_2$ is 5.6 nm. The diffusion length (standard deviation) amounts about 2 nm for T = 700 °C and therefore a more advanced treatment has to be used to get the O diffusivity. The χ^2 value of the description of the experiment is determined as a function of *Dt*, and in this way the *Dt* value that describes the experiment best is determined (see insert). The red line corresponds to the best fit using of the value diffusion parameter *Dt* that it is distinct for each temperature used. The optimum *Dt* value was determined from the minimum of the χ^2 function for 600, 700 and 800°C as shown in the insets of Fig. 5 and corresponds to approximately 0.28, 0.68 and 2.98 nm^2, respectively.

The relationship between the calculated diffusivity for each annealing temperature is observed in the Arrhenius plot of Fig. 6. The activation energy for oxygen self-diffusion amounts to 1.09 ± 0.16 eV and the uncertainty accounts for the fitting procedure and error bars. The present activation energy is consistent with results obtained elsewhere for similar sputter-deposited samples (1.05 eV) [1]. In Ref. [1] it was also shown that the diffusion was not regular, i.e. additional annealing at the same temperature resulted in only very modest increases of the obtained *Dt* value, suggesting that defects initially present in the TiO_x layer play a role. Indeed the O diffusion in single crystal rutile samples show much smaller self-diffusion values [1].

4. Conclusion

The nuclear reaction $^{18}O(p,\alpha)^{15}N$ at 151 keV allows oxygen self-diffusion measurements across oxides applied for ReRAM memory devices. This technique was demonstrated to be able to determine the ^{18}O depth distribution with a resolution of several nm. We successfully measured the activation energy for the oxygen self-diffusion without removing the (Si_3N_4) cap layer. It amounts approximately 1 eV, which is consistent with values obtained by ERBS measurements for similar sputter-deposited samples.

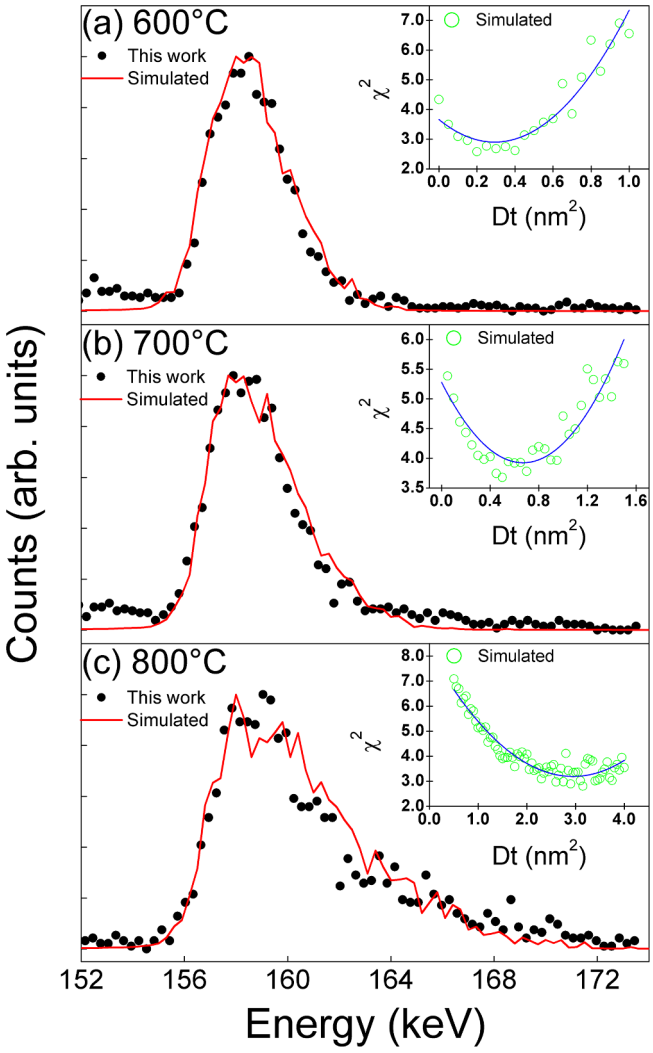

Fig. 5. Experimental excitation curves and fitting for sample D annealed at (a) 600 °C, (b) 700 °C and (c) 800 °C. The insets show the corresponding χ^2 values of the fit versus *Dt* value assumed for each simulation.

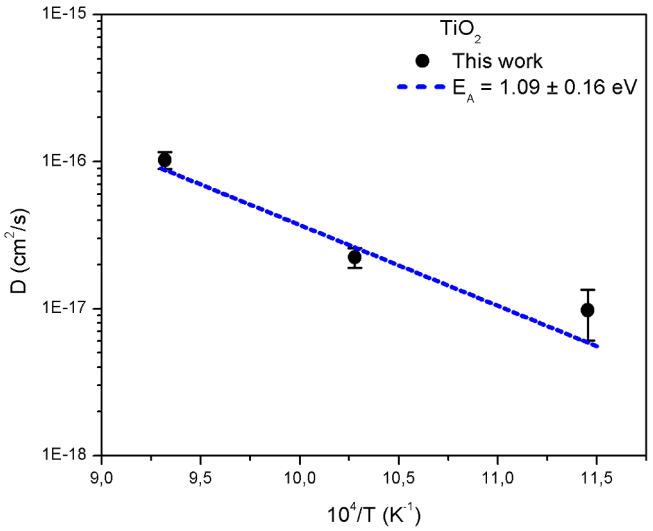

Fig. 6. Arrhenius plot for three annealing temperatures.

Acknowledgement

This study was financed in part by the Coordena de Aperfei oamento de Pessoal de Nvel Superior – Brasil (CAPES) – Finance Code 001, by CNPq and PRONEX-FAPERGS. We acknowledge support from the NCRIS ANFF and Heavy-Ion Accelerator Capabilities, with particular thanks to Dr. Fouad Karouta for the deposition of the (Si_3N_4) at ANU. RGE and MV further acknowledge the ARC funding program for financial support.

References

[1] G. Marmitt, S. Nandi, D. Venkatachalam, R. Elliman, M. Vos, P. Grande, Oxygen diffusion in TiO2 films studied by electron and ion Rutherford backscattering, Thin Solid Films 629 (2017) 97–102.
[2] R. Waser, M. Aono, Nanoionics-based resistive switching memories, Nat. Mater. 6 (11) (2007) 833.
[3] A. Sawa, Resistive switching in transition metal oxides, Mater. Today 11 (6) (2008) 28–36.
[4] D. Ielmini, F. Nardi, C. Cagli, Universal reset characteristics of unipolar and bipolar metal-oxide RRAM, IEEE Trans. Electron Devices 58 (10) (2011) 3246–3253.
[5] I. Baumvol, Atomic transport during growth of ultrathin dielectrics on silicon, Surf. Sci. Rep. 36 (1–8) (1999) 1–166.
[6] G. Copetti, G.V. Soares, C. Radtke, Stabilization of the GeO2/Ge interface by nitrogen incorporation in a one-step no thermal oxynitridation, ACS Appl. Mater. Interfaces 8 (40) (2016) 27339–27345.
[7] C. Driemeier, L. Miotti, R. Pezzi, K. Bastos, I. Baumvol, The use of narrow nuclear resonances in the study of alternative metal-oxide-semiconductor structures, Nucl. Instrum. Methods Phys. Res., Sect. B 249 (1–2) (2006) 278–285.
[8] J.R. Tesmer, M. Nastasi, Handbook of modern ion beam materials analysis, Materials Research Society, 9800 McKnight Rd, Suite 327, Pittsburgh, PA 15237, USA, 1995. 700.
[9] Y. Wang, M.A. Nastasi, Handbook of Modern Ion Beam Materials Analysis, Materials Research Society Warrendale, Pennsylvania, 2009.
[10] M.D.A. Sortica, P.L. Grande, G. Machado, L. Miotti, Characterization of nanoparticles through medium-energy ion scattering, J. Appl. Phys. 106 (11) (2009) 114320 .
[11] G.G. Marmitt, PowerMEIS simulation code,http://tars.if.ufrgs.br/.
[12] K.J. Mighell, Parameter estimation in astronomy with poisson-distributed data. I. The χ^2_γ statistic, Astrophys. J. 518 (1) (1999) 380.
[13] J.F. Ziegler, SRIM-2003, Nucl. Instrum. Methods Phys. Res. Section B 219 (2004) 1027–1036.
[14] W.K. Chu, J.W. Mayer, M.A. Nicolet, Backscattering Spectrometry, Academic Press, 1987.